Northern Hemisphere Stratospheric Pathway of Different El Niño Flavors in Stratosphere-Resolving CMIP5 Models

N. Calvo,[a] M. Iza,[a] M. M. Hurwitz,[b,c,j] E. Manzini,[d] C. Peña-Ortiz,[e] A. H. Butler,[f]
C. Cagnazzo,[g] S. Ineson,[h] and C. I. Garfinkel[i]

[a] *Departamento Fisica de la Tierra II, Universidad Complutense de Madrid, Madrid, Spain*
[b] *NASA Goddard Space Flight Center, Greenbelt, Maryland*
[c] *Goddard Earth Sciences Technology and Research, Morgan State University, Baltimore, Maryland*
[d] *Max Planck Institute for Meteorology, Hamburg, Germany*
[e] *Universidad Pablo de Olavide, Sevilla, Spain*
[f] *Chemical Sciences Division, NOAA/ESRL, and CIRES, Boulder, Colorado*
[g] *Instituto di Fisica dell'Atmosfera e del Clima, Consiglio Nazionale delle Ricerche, Rome, Italy*
[h] *Met Office Hadley Centre, Exeter, United Kingdom*
[i] *Fredy and Nadine Herrmann Institute of Earth Science, Hebrew University, Jerusalem, Israel*

ABSTRACT

The Northern Hemisphere (NH) stratospheric signals of eastern Pacific (EP) and central Pacific (CP) El Niño events are investigated in stratosphere-resolving historical simulations from phase 5 of the Coupled Model Intercomparison Project (CMIP5), together with the role of the stratosphere in driving tropospheric El Niño teleconnections in NH climate. The large number of events in each composite addresses some of the previously reported concerns related to the short observational record. The results shown here highlight the importance of the seasonal evolution of the NH stratospheric signals for understanding the EP and CP surface impacts. CMIP5 models show a significantly warmer and weaker polar vortex during EP El Niño. No significant polar stratospheric response is found during CP El Niño. This is a result of differences in the timing of the intensification of the climatological wavenumber 1 through constructive interference, which occurs earlier in EP than CP events, related to the anomalous enhancement and earlier development of the Pacific–North American pattern in EP events. The northward extension of the Aleutian low and the stronger and eastward location of the high over eastern Canada during EP events are key in explaining the differences in upward wave propagation between the two types of El Niño. The influence of the polar stratosphere in driving tropospheric anomalies in the North Atlantic European region is clearly shown during EP El Niño events, facilitated by the occurrence of stratospheric summer warmings, the frequency of which is significantly higher in this case. In contrast, CMIP5 results do not support a stratospheric pathway for a remote influence of CP events on NH teleconnections.

1. Introduction

In the last decade, a robust impact of the warm phase of El Niño–Southern Oscillation (ENSO) has become evident in the Northern Hemisphere (NH) polar stratosphere. Although ENSO is an ocean–atmosphere coupled phenomenon that takes place in the tropical Pacific Ocean, it impacts global climate. During the warm ENSO phase (here referred to as El Niño), its signal extends from the tropics to the extratropics by means of atmospheric Rossby wave trains, associated with an anomalous Pacific–North American (PNA) pattern in the NH during winter. These Rossby waves can also propagate upward and reach the stratosphere (e.g., García-Herrera et al. 2006) through the deepening of the Aleutian low in the PNA pattern and enhancement of wavenumber 1 (Manzini et al. 2006; Garfinkel and Hartmann 2008). As waves dissipate at middle and high latitudes in the stratosphere, they lead to a weaker polar vortex and a strengthening of the Brewer–Dobson circulation during El Niño. This strengthening generates anomalous cooling in the tropical stratosphere and anomalous warming in the polar stratosphere

[j] Current affiliation: Science Systems and Applications, Inc., Lanham, Maryland.

Corresponding author e-mail: N. Calvo, nataliac@fis.ucm.es

(Sassi et al. 2004; García-Herrera et al. 2006; Manzini et al. 2006). A robust El Niño signal in polar stratospheric temperatures has also been found in radiosondes (Free and Seidel 2009) and satellite data (Cagnazzo et al. 2009), in agreement with the mechanism first proposed in modeling studies and reanalysis data. An El Niño impact on the Arctic polar ozone has also been reported based on observations and general circulation models (Cagnazzo et al. 2009), consistent with enhanced downwelling over the Arctic.

El Niño modulation of the NH polar vortex can have an effect higher up in the mesosphere (Li et al. 2013) and also impact lower levels, reaching the troposphere. Weaker vortex anomalies have been shown to descend into the troposphere during El Niño events, contributing to a negative Arctic Oscillation (AO) phase and affecting surface climate in the NH region. In fact, several studies have highlighted the active role of the polar stratosphere in driving tropospheric teleconnections in the North Atlantic European (NAE) region and suggest that major stratospheric sudden warmings (SSWs) may modulate the downward propagation of the signals (e.g., Ineson and Scaife 2009; Cagnazzo and Manzini 2009; Bell et al. 2009; Butler et al. 2014).

Recent studies have pointed out the importance of distinguishing different "flavors" of ENSO. They have revealed a different type of event characterized by the largest sea surface temperature (SST) anomalies located in the central tropical Pacific. Its warm phase is known as central Pacific El Niño, warm pool El Niño, date line El Niño, or El Niño Modoki (Ashok et al. 2007; Yeh et al. 2009; Kao and Yu 2009; Kug et al. 2009; Larkin and Harrison 2005), while the traditional El Niño, with the largest SST anomalies in the eastern Pacific, is referred as canonical El Niño, eastern Pacific El Niño, or cold tongue El Niño. Here we will use central Pacific (CP) El Niño and eastern Pacific (EP) El Niño to denote these two types of warm ENSO events.

The different locations of the SST anomalies in CP and EP El Niño lead to distinct tropospheric teleconnection patterns (Weng et al. 2007, 2009; Kao and Yu 2009; Kim et al. 2009). In the stratosphere, CP El Niño has a clear impact on the Southern Hemisphere (SH) polar lower-stratospheric region in the form of an anomalous significant warming, absent during EP El Niño (Hurwitz et al. 2011a,b; Zubiaurre and Calvo 2012; Xie et al. 2012). This response is related to an intensified Pacific–South American (PSA) pattern due to enhanced tropical convection west and south of the date line (Hurwitz et al. 2011a; Zubiaurre and Calvo 2012).

In the Northern Hemisphere, the CP El Niño impact on the polar stratosphere is not as clear as in the SH, and contradictory results have been reported. On the one

hand, Hegyi and Deng (2011) found a significantly stronger polar vortex in MERRA during CP El Niño. This signal in wind was consistent with that reproduced in temperature with a climate model, although it was found not significant (Zubiaurre and Calvo 2012). On the other hand, Graf and Zanchettin (2012), Garfinkel et al. (2013), and Hegyi et al. (2014) reported an anomalously weak polar vortex in CP El Niño in reanalysis data and two idealized simulations, respectively. However, in the NCEP–NCAR reanalyses data, Sung et al. (2014) found a weaker polar vortex during CP events only in the upper stratosphere. In the middle and lower polar stratosphere, the CP El Niño response was mainly negligible. Interestingly, the characterization of specific winters as EP or CP does differ among these studies. Garfinkel et al. (2013) compared several of the definitions used to characterize CP El Niño events and concluded that, at least in reanalysis data, the NH polar stratospheric response to CP El Niño was not robust, as its sign depended on the composite size, the index used, and the month or seasonal average analyzed. Very recently, Iza and Calvo (2015) highlighted the role of SSWs in the characterization of the CP El Niño response in reanalysis data. They showed that the CP El Niño response in the NH polar stratosphere depended on the occurrence of SSWs such that, in the absence of SSWs, CP and EP El Niño responses were opposite in the polar stratosphere. Furthermore, the different responses reported during CP events in the polar stratosphere may lead to different signals in the tropospheric teleconnection over the NAE region, as was shown in several studies based on reanalysis data (e.g., Hegyi and Deng 2011; Sung et al. 2014). It is therefore clear that the impacts of EP and CP El Niño on the NH polar stratosphere and NH climate still deserve further investigation.

Model simulations from the CMIP5 activity provide ensembles large enough to investigate ENSO signals in depth. Kim and Yu (2012) and Kug et al. (2012) showed that CMIP5 models tend to simulate more independent EP and CP El Niño patterns compared to CMIP3 models. In this regard, CMIP5 models constitute the first opportunity to analyze the stratospheric response of EP and CP El Niño in ocean–atmosphere coupled models with a well-resolved stratosphere (Gerber et al. 2012; Charlton-Perez et al. 2013). Cagnazzo et al. (2009) analyzed the NH ENSO signal in the Chemistry–Climate Model Validation Activity, version 2 (CCMVal2), multimodel ensemble, which included atmospheric general circulation models (mostly high top), not coupled to the ocean, but driven with observed SSTs and sea ice concentrations as boundary conditions. They reported a robust El Niño signal in the NH polar

TABLE 1. CMIP5 high-top models used in the study.

Models	Resolution[a] (Lon × Lat)	Levels	Top	SSWs frequency
CESM1(WACCM)	144 × 96	66	5.96×10^{-6} hPa	0.63
CMCC-CESM	144 × 96	39	0.01 hPa	0.54
CMCC-CMS	192 × 96	95	0.01 hPa	0.69
CanESM2	128 × 64	35	1 hPa	1.15
GFDL CM3	144 × 90	48	0.01 hPa	0.30
HadGEM2-CC	192 × 145	60	85 km	0.57
MIROC-ESM	128 × 64	80	0.0036 hPa	0.65
MIROC-ESM-CHEM	128 × 64	80	0.0036 hPa	0.61
MPI-ESM-LR	192 × 96	47	0.01 hPa	0.81
MPI-ESM-MR	192 × 96	95	0.01 hPa	0.87
MRI-CGCM3	320 × 160	48	0.01 hPa	0.31

[a] Resolution is given as number of grid points.

stratosphere, in agreement with observations, but did not explore the differences between EP and CP El Niño. Hurwitz et al. (2014) did investigate the atmospheric response to EP and CP ENSO in the CMIP5 models from a seasonal-mean point of view and found indistinguishable winter-mean responses to EP and CP El Niño in the NH polar stratosphere at 50 hPa. The stratospheric vortex weakened for both types of El Niño although there was substantial intermodel variability. However, several studies have emphasized the importance of studying the seasonal evolution of El Niño response from early to late winter/early spring (e.g., Manzini et al. 2006; Ineson and Scaife 2009; Fletcher and Kushner 2011; Sung et al. 2014), which is key for depicting 1) upward wave propagation from the troposphere to the stratosphere, 2) wave–mean flow interactions and nonlinear interactions between ENSO and other sources of stratospheric variability (Calvo et al. 2009; Calvo and Marsh 2011), and 3) the potential downward stratosphere to troposphere coupling. While the seasonal evolution of the EP El Niño response has been previously investigated, most of the studies regarding CP El Niño in the NH have focused on seasonal means. In addition, the signal of El Niño in the stratosphere can be influenced by other sources of variability, such as the quasi-biennial oscillation or solar variability (e.g., Calvo et al. 2009; Calvo and Marsh 2011; Richter et al. 2015). While the analysis of the influence of these signals on the El Niño response is out of the scope of this paper, the approach followed here using large ensembles with El Niño cases from many different models with different configurations helps to focus on the El Niño signal and minimize the influence of other phenomena.

Thus, our study constitutes the first attempt to investigate the seasonal evolution of the NH stratospheric responses to EP and CP El Niño events in an ensemble of atmosphere–ocean coupled simulations from different models with a well-resolved stratosphere. We explore the

similarities and differences between EP and CP signals with the aim of understanding contradictory previous results. The role of the stratosphere in driving the tropospheric ENSO–NAE teleconnections is also assessed. Since stratospheric variability is poorly represented in low-top CMIP5 models (Charlton-Perez et al. 2013) and Hurwitz et al. (2014) argued that ENSO-related polar variability was better simulated in the high-top CMIP5 group of models (those with a model lid above 1 hPa; Charlton-Perez et al. 2013), our study analyzes models of this group exclusively.

2. Models and method

Table 1 lists the 11 CMIP5 high-top models used in this study. They are all atmosphere–ocean coupled models with the model lid above 1 hPa. Note that they do not exactly coincide with the group of high-top models analyzed by Charlton-Perez et al. (2013). In particular, the IPSL and NASA GISS high-top models are not included in our study, as data above 10 hPa were not provided to the CMIP5 archive at the time of the analysis. Simulations from historical experiments (Taylor et al. 2012) from 1951 to 2005 have been analyzed and only one ensemble member per model for each experiment has been used. The historical simulations are run with observed climate forcings (including greenhouse gas concentrations, ozone depletion, aerosols, land-use change, and solar variability).

EP and CP El Niño events are defined based on the standardized detrended November–February (NDJF) SST anomalies in the regions of Niño-3 (N3; 5°N–5°S, 150°–90°W) and Niño-4 (N4; 5°N–5°S, 160°E–150°W), respectively. We adopt this simple definition in the interest of clarity. As in Hurwitz et al. (2014), EP El Niño winters are identified when the anomalies in the N3 index are larger than one standard deviation and exceed the value of the N4 index by at least 0.1. Analogously, CP El

TABLE 2. Number of El Niño events included in the composites.

EP El Niño			CP El Niño		
All	With SSWs	Without SSWs	All	With SSWs	Without SSWs
48	32	16	43	20	23

Niño winters are identified when the anomalies of the N4 index are larger than one standard deviation and exceed the N3 value by at least 0.1. In this fashion, the same winter cannot be considered as both EP and CP El Niño. A total of 48 EP events and 43 CP events are identified from the 11 historical simulations (see Table 2). While the frequency of EP events agrees well with that from reanalysis, CMIP5 models tend to underestimate the observed number of CP El Niño (Bellenguer et al. 2014).

The EP and CP El Niño signals are then analyzed by compositing, for each field, monthly mean anomalies for all the El Niño events identified across all models. Anomalies for each field are computed with respect to their own 55-yr model climatologies. For each model, time series of historical simulations are detrended before computing the anomalies. Significance of the El Niño anomalies is assessed at the 95% confidence level by a Monte Carlo test of 1000 trials. Random groups of 48 and 43 events are composited from the entire pool of anomalies from all the years and all the models to be compared with the EP and CP composites. The significant signals discussed here show agreement in the sign of the anomaly in at least 70% of the models (8 out of 11 models).

To quantify the role of linear interference between the climatological stationary fields and the forced El Niño waves, we have followed the methodology described in Smith et al. (2010) and Fletcher and Kushner (2011) using daily data. The El Niño composite anomalous meridional eddy heat flux is decomposed as in Eq. (1), where v is the meridional wind component and T is temperature. Asterisks denote the deviation with respect to the zonal mean (the eddy), angle brackets denote the ensemble mean (EM), c denotes the climatological mean, and a denotes the deviation from the climatological mean (El Niño anomalies). The linear interference effect (which will be the focus of our study) appears in the $\mathrm{EM_{LIN}}$ term, while the $\mathrm{EM_{NL}}$ accounts for the anomalous eddy heat flux associated with the wave itself. The fluctuation (FL) term is calculated as the residual and it includes the inter-ensemble and transient eddy contributions:

$$\langle (v^*T^*)_a \rangle = \mathrm{EM_{LIN}} + \mathrm{EM_{NL}} + \mathrm{FL}, \quad \text{where}$$
$$\mathrm{EM_{LIN}} = \langle T_a^* \rangle \langle v_c^* \rangle + \langle v_a^* \rangle \langle T_c^* \rangle \quad \text{and}$$
$$\mathrm{EM_{NL}} = \langle v_a^* \rangle \langle T_a^* \rangle. \tag{1}$$

Note that, in our study, the El Niño anomalies are computed with respect to their own 55-yr model climatology, while the climatological mean is the mean of all the years in all the models (which agrees well with the climatology of individual models).

Daily CMIP5 output is also used to identify SSW events. SSWs are identified following the definition of Charlton and Polvani (2007): a major SSW occurs when the zonal-mean zonal winds at 60°N and 10 hPa change from westerly to easterly between the months of November and March. Winds must return to westerly for at least 20 consecutive days between events and for 10 consecutive days before 30 April. For each model, the SSW frequency of occurrence is computed considering 1951–2005 and is reported in Table 1. With the exception of HadGEM2-CC, our frequencies compare well with those reported by Charlton-Perez et al. (2013). Given that we use a longer period (1951–2005), instead of 1960–2000 as in Charlton-Perez et al. (2013), our estimates may differ from those of Charlton-Perez et al. (2013) and are possibly more robust. The multimodel mean of our simulations reproduces the observed frequency of the SSWs, although there is quite a large spread in the simulated frequencies for individual models, ranging from 0.3 to 1.1 events per year (Table 1). Still, in most of the models, their frequency agrees with observations within the 95% confidence level.

3. Tropospheric teleconnections associated with El Niño

Figure 1 shows the spatial pattern of sea surface temperature in the tropical Pacific Ocean composited for the EP and CP El Niño events. The warm anomalies peak in the eastern Pacific in EP El Niño, while during CP El Niño the largest warming is simulated around the date line. In addition, EP El Niño warming extends southward along the coast of South America while the CP El Niño anomalies are much weaker therein. These patterns are in good agreement with observations [e.g., Fig. 1 in Kim and Yu (2012)], despite some differences (the modeled CP anomalies extend southeastward toward the coast more than in the observations in late winter, while the EP anomalies might not extend far enough southeast). Note also that, as in the observations, the overall amplitude of the warming is higher in EP El Niño than in CP El Niño, even though CMIP5 models still underestimate the amplitudes of the largest EP El Niño events (Kim and Yu 2012). In terms of seasonality, the largest anomalies are simulated from November to February in both EP and CP events (not shown). Thus, potential differences in the atmospheric response cannot be attributed to differences in the

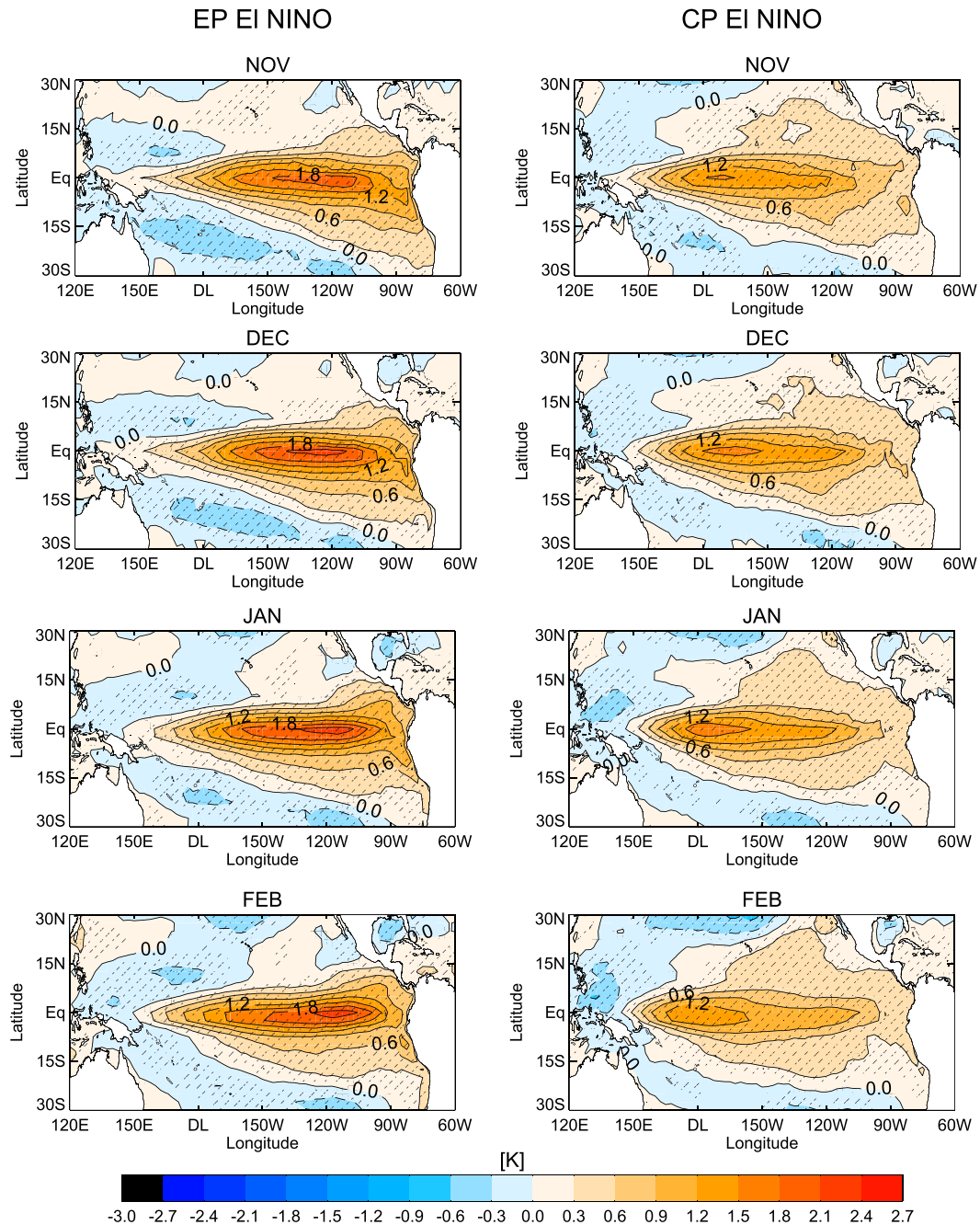EP El NINO   CP El NINO

FIG. 1. Longitude–latitude composite of SST anomalies (K) for (left) EP El Niño and (right) CP El Niño from November to February. Contour interval is 0.3 K. Solid (dashed) contours denote positive (negative) anomalies. Stippling indicates significance at the 95% confidence level.

timing of occurrence of the events. Overall, this comparison gives us confidence to investigate the differences in their atmospheric response between the two types of ENSO events.

El Niño tropospheric teleconnection patterns in the NH are displayed in Fig. 2 by means of the EP and CP El Niño composites of eddy geopotential height

anomalies at 500 hPa. This is a common diagnostic used in the literature to explore the ENSO modulation of the PNA pattern. The PNA response (e.g., Wallace and Gutzler 1981) is characterized by an anomalous low in the North Pacific Ocean, an anomalous high in the northern United States and Canada, and an anomalous low over the Gulf of Mexico. It appears significant in
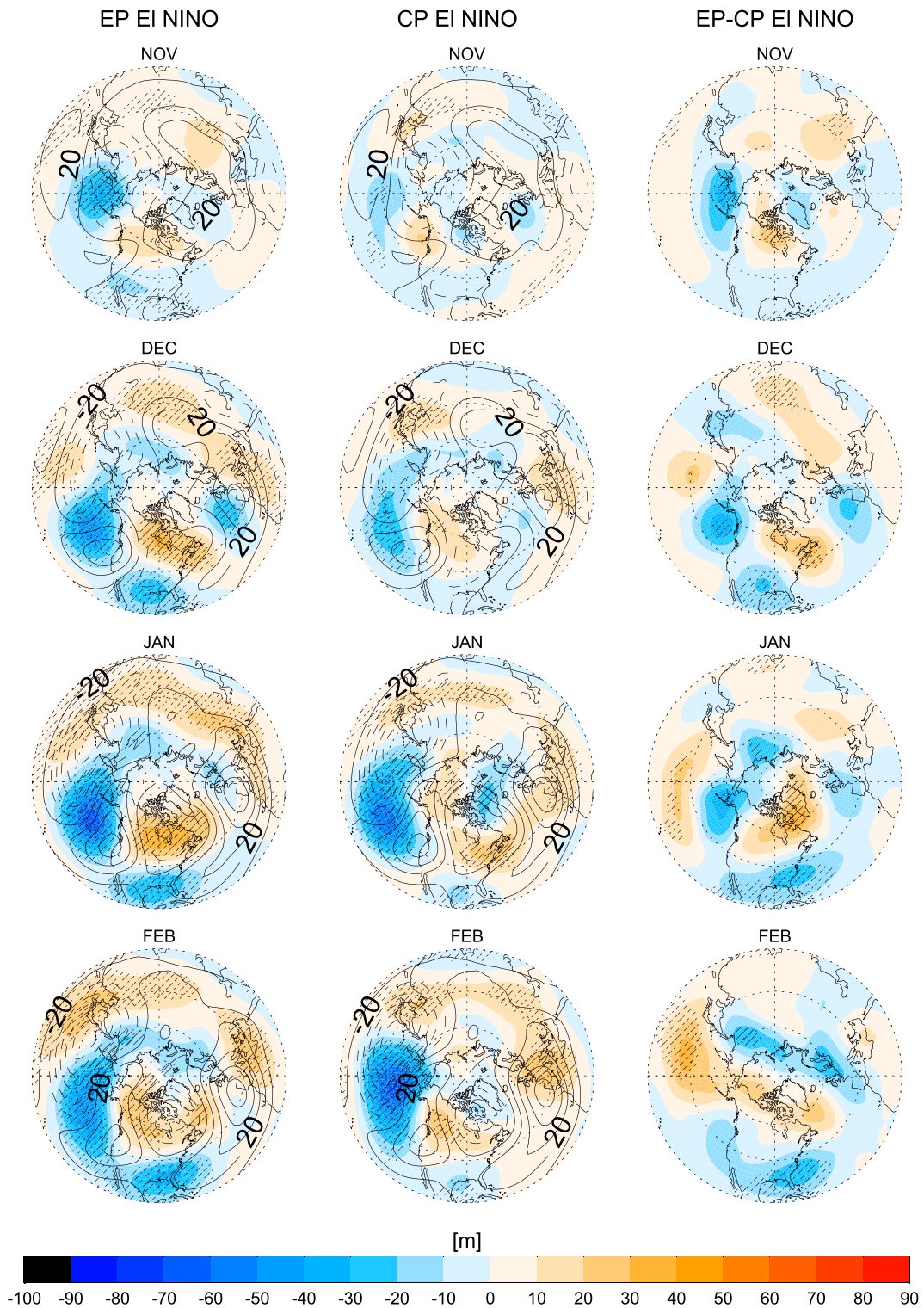
FIG. 2. Composite of the 500-hPa eddy geopotential height anomalies (m; color shading) for (left) EP El Niño, (center) CP El Niño, and (right) the difference between EP and CP together with the multimodel mean climatology (contours) from November to February. Color interval is 10 m. Solid (dashed) contours, every 20 m, denote positive (negative) values. Stippling indicates significance at the 95% confidence level.

both EP and CP El Niño composites, although the pattern is more coherent and stronger during EP El Niño events. Garfinkel et al. (2010) showed that, in observations, the deepening of the Aleutian low was key to modulating the polar vortex in response to ENSO. A significant deepening of the Aleutian low is seen from November to February during EP events and, later in the season, from December to February, in CP events. The deepening is stronger and extends northward in EP El Niño from November to January (significant differences between EP and CP El Niño at the 95% confidence level; Fig. 2, right), whereas the magnitude and location are similar in February. The more northward extension of the Aleutian low during EP events seems to be a seasonal feature, as it also appears in the seasonal mean of the high-top CMIP5 models reported by Hurwitz et al. (2014; their Fig. 1). The CMIP5 behavior is in agreement with previous studies that used reanalysis data and single-model simulations. In reanalysis data, Yu and Kim (2011) and Sung et al. (2014) found a delayed PNA response to the SST anomalies and, in particular, a weaker and less immediate response of the deepening of the Aleutian low in CP El Niño events compared to EP El Niño. The more northward displacement of the Aleutian low in EP El Niño events and the similar response between EP and CP events in late winter were also reported in Goddard Earth Observing System Chemistry–Climate Model (GEOSCCM) simulations (Garfinkel et al. 2013).

In addition to the Aleutian low, clear differences in the anomalous high center of the PNA over the northeastern United States and Canada are also found between EP and CP El Niño in Fig. 2. Larger anomalies, significant over larger areas and elongated toward the Atlantic, are simulated during EP El Niño. Although the deepening of the Aleutian low has received most of the attention as a precursor of polar vortex weakening, Garfinkel et al. (2010) also identified the positive anomaly in geopotential height over the regions of northeastern Canada and the North Atlantic as an important factor for wave driving into the stratosphere (see their Fig. 3c). Thus, differences between EP and CP El Niño found in this region (significant at the 95% level from November to January; Fig. 2, right) also trigger differences in the stratospheric response, as will be shown in section 5.

4. Upward propagation of El Niño signal into the stratosphere

As discussed in the introduction, the canonical El Niño signal on the PNA propagates upward into the stratosphere during boreal winter by means of Rossby waves (e.g., García-Herrera et al. 2006). This is

hypothesized to occur through constructive interference between the El Niño eddy anomalies and the climatological eddy fields (Fletcher and Kushner 2011), mainly associated with wavenumber 1 (abbreviated as wave1) (e.g., Manzini et al. 2006; Garfinkel and Hartmann 2008). Figure 3 shows a vertical cross section of the longitudinal distribution of the wave1 eddy geopotential height anomalies averaged over 45°–75°N during El Niño events, superimposed on the multimodel mean climatology. CMIP5 models clearly simulate a significant enhancement of the climatological wave1 during EP events from November to January, as the anomalies are in phase with the climatology. During CP El Niño, tropospheric anomalies are weak in early winter, in agreement with the weak PNA pattern shown in these months in Fig. 2. Only in February do CP El Niño anomalies seem to be in phase with the climatological patterns. Note that both negative anomalies in the northern Pacific Ocean (Aleutian low) around the date line and positive anomalies over the eastern part of North America and the western Atlantic Ocean (west of 60°W) are important in enhancing the climatological wave1 pattern in the troposphere. Regarding wavenumber 2 (abbreviated as wave2; not shown), models simulate a significant weakening of the climatological pattern from December to February during both EP and CP events, although the magnitude of the anomalies is half of that of wave1. The wave2 weakening during EP events was already shown in other single-model studies (Taguchi and Hartmann 2006; Li and Lau 2013).

In addition to the EP and CP geopotential height anomalies in wave1 amplitude shown in Figs. 3 (left and center), Fig. 3 (right) shows the corresponding EP and CP wave1 geopotential height phase anomaly computed from November to February and the 45°–75°N average. The anomalies are computed as the phase difference between the eddy El Niño anomalies and the eddy multimodel mean climatology. Results show that the EP anomaly and the climatology are in phase from November to January from the midtroposphere to the upper stratosphere [as the phase difference is comprised between 90° and −90°; see Smith and Kushner (2012) for more details]. In contrast, for CP events, a clear in-phase behavior only appears in February. These results corroborate visual inspection of the behavior of the wave amplitudes during El Niño events with respect to the climatology (Figs. 3, left and center).

Results from Fig. 3 suggest differences in the upward propagation of wave1 through changes in wave interference between the EP and CP anomalies and the climatological field. Linear interference between the climatological and the anomalous El Niño wave1 can be quantified by computing the linear term of the
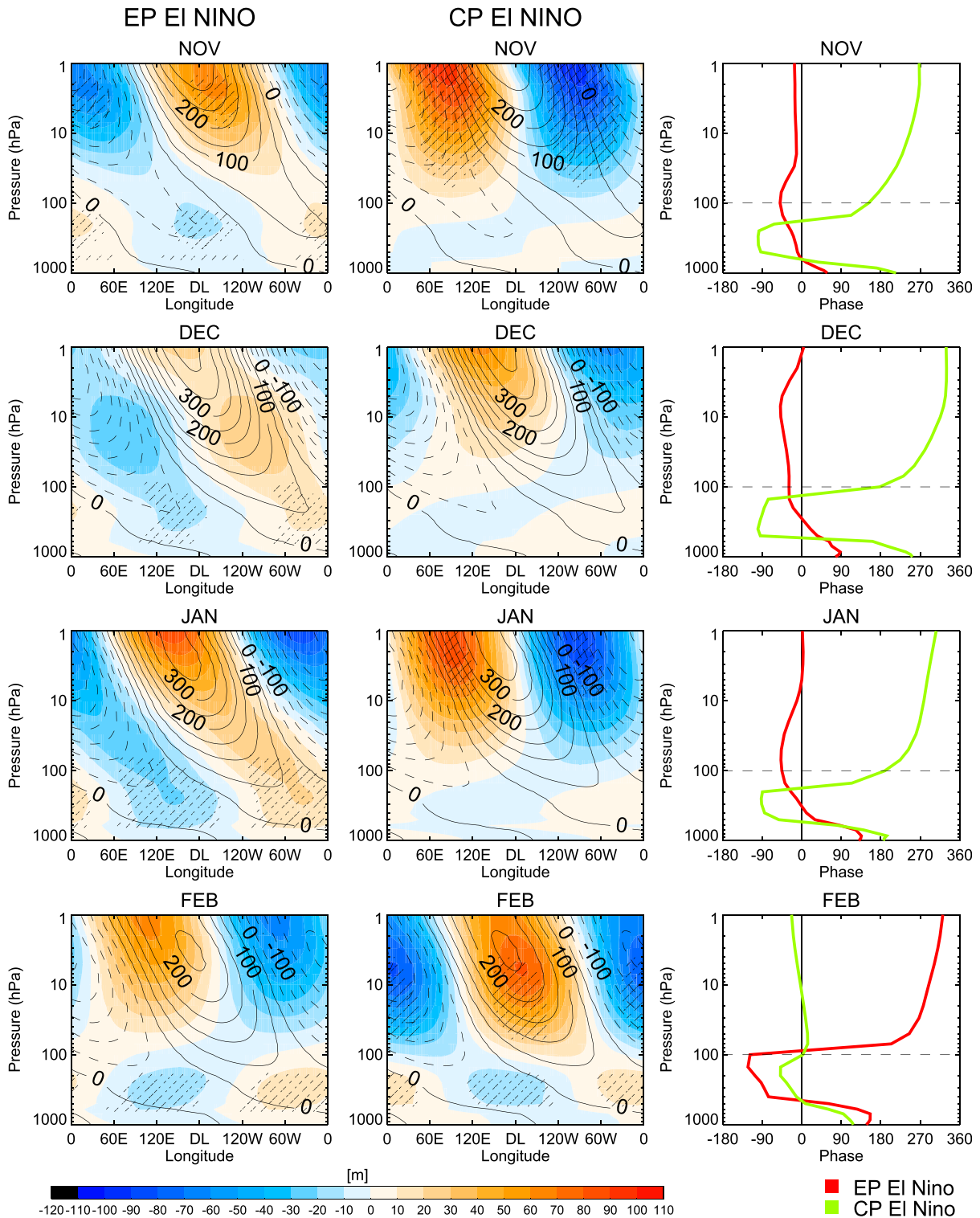
FIG. 3. Longitude–pressure cross sections of wave1 geopotential height anomalies (color shading) composited for (left) EP El Niño and (center) CP El Niño, averaged from 45° to 75°N. Solid (dashed) line contours, every 50 m, denote positive (negative) values of the multimodel mean climatology. See more details in the text. Stippling indicates significance at the 95% confidence level. (right) Vertical evolution of the phase difference between the anomalous El Niño wave1 and the climatological wave1 [following Smith and Kushner (2012); their Fig. 5].
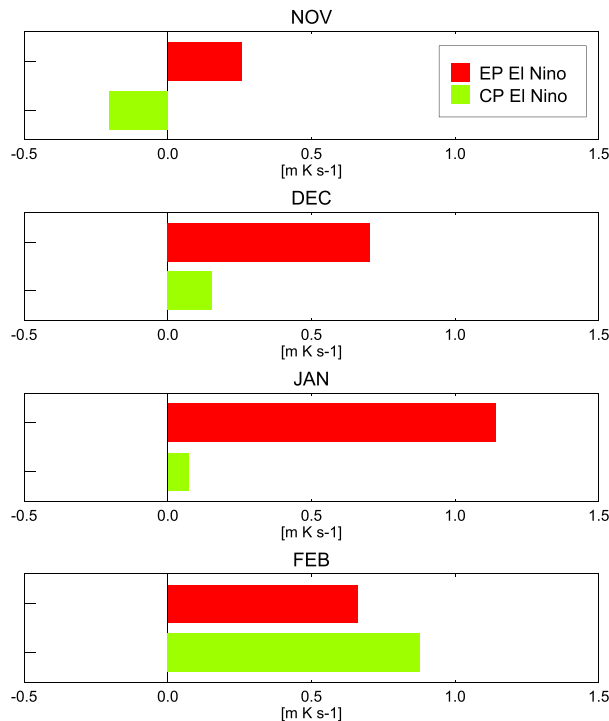
FIG. 4. Linear term [as in Eq. (1)] of the anomalous eddy meridional heat flux [as in Eq. (1)] for EP El Niño (red) and CP El Niño (green) from November to February at 100 hPa.

TABLE 3. Total anomalous meridional wavenumber-1 eddy heat flux values at 100 hPa and averaged over 45°–75°N and their decomposition in different terms according to Smith et al. (2010) and Fletcher and Kushner (2011) from November to February for EP and CP El Niño events.

	Nov	Dec	Jan	Feb
EP events				
Total	0.24	0.69	0.31	0.13
EM_{LIN}	0.26	0.70	1.15	0.66
EM_{NL}	0.04	0.10	0.22	0.11
FL	−0.06	−0.11	−1.04	−0.64
CP events				
Total	0.29	0.38	0.29	0.64
EM_{LIN}	−0.20	0.15	0.07	0.88
EM_{NL}	−0.01	0.04	0.03	0.13
FL	0.50	0.19	0.19	−0.37

meridional eddy heat flux (i.e., EM_{LIN}), as described in section 2, Eq. (1) (Smith et al. 2010; Fletcher and Kushner 2011). Figure 4 shows this term at 100 hPa, averaged from 45° to 75°N from November to February for EP and CP events. (Similar results are found at 50 hPa.) The analysis of all the terms in Eq. (1) is shown in Table 3. It reveals that the interference term computed here (i.e., EM_{LIN}) dominates over the nonlinear (i.e., EM_{NL}) term in all the months for both EP and CP El Niño events. The EM_{LIN} term is also larger than the fluctuation term (i.e., FL) in the months in which the values of the total anomalous eddy heat flux are the largest (November and December in EP events and February in CP events). Interestingly, the compensation between the linear term and the fluctuation term in the EP case in January and February supports the idea that the coupling in early winter is primarily upward while later in the winter there is more downward influence, as we will show in section 5. In the CP case, the fluctuation term is larger (in absolute value) than the EM_{LIN} term from November to January, indicating that during most of the winter the interensemble and transient variability dominates over the signal from a forced response.

Figure 4 shows that, during EP events, the linear term of the anomalous meridional eddy heat flux is always positive, indicating constructive interference. It reaches the largest value in January, in agreement with Fig. 3. During CP events, the wave1 anomalous meridional eddy heat flux is negative in November (indicating destructive interference) and almost negligible in December and January. Only in February are large values of the anomalous meridional wave1 eddy heat flux simulated at 100 and 50 hPa larger than those for EP events, indicating constructive interference. These results corroborate those from visual inspection of Fig. 3 and highlight the differences between EP and CP events in upward propagation through constructive interference between the eddies and the climatology.

In summary, the CMIP5 models simulate distinct seasonal evolutions of the upper-tropospheric responses to EP and CP El Niño events, with the CP events lagging behind by about two months. During EP events, the deepening of the Aleutian low extends toward northern latitudes, and the intensification of the high in the northern part of North America is stronger and occurs earlier in the season compared to CP El Niño. This tropospheric response translates into a significant wave1 intensification in phase with the wave1 climatology in midwinter from November to January. During CP events, the deepening of the Aleutian low occurs later in the season, and the enhancement of the high over North America is weaker and does not extend toward the Atlantic in early winter. As a result, the in-phase intensification of wave1 with the climatology appears only in February.

5. Stratospheric response and downward propagation of El Niño signals at high latitudes: Influence of stratospheric sudden warmings

Next, we will show how the differences in the timing of the responses revealed in the previous section affect the zonal-mean stratospheric EP and CP El Niño signals. Figures 5 and 6 show the latitude–altitude cross section
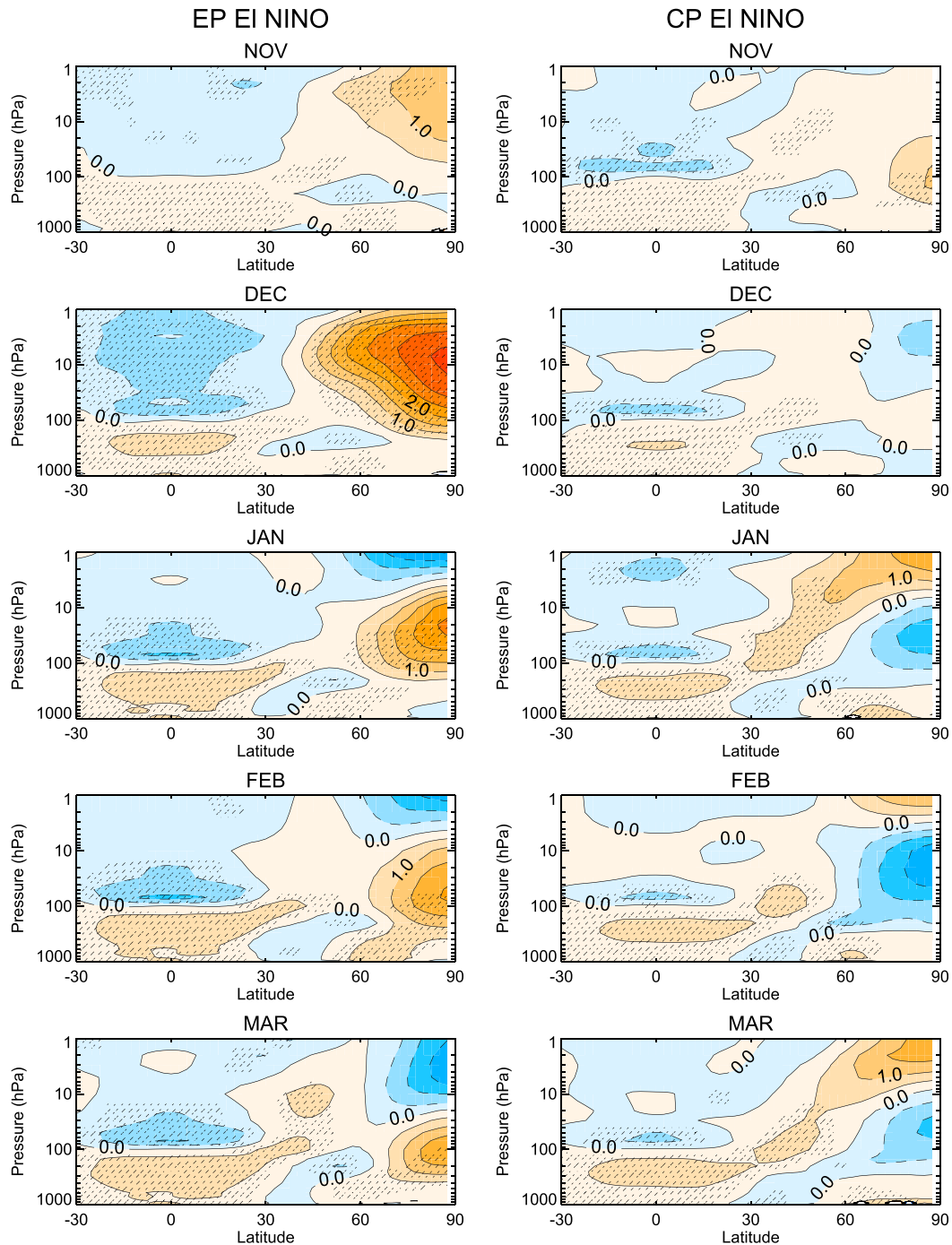
FIG. 5. Latitude–pressure cross sections of zonal-mean temperature anomalies (K) composited for (left) EP El Niño and (right) CP El Niño from November to March. Contour interval is 0.5 K. Solid (dashed) contours denote positive (negative) anomalies. Stippling indicates significance at the 95% confidence level.

of El Niño composites of zonal-mean temperature and zonal-mean zonal wind anomalies, respectively. In the tropical troposphere, a significant zonal-mean warming (Fig. 5) is simulated in response to the anomalies in SST, larger in EP El Niño than in CP El Niño, and in

agreement with observations (e.g., Calvo Fernández et al. 2004; Free and Seidel 2009). These anomalies are accompanied by an intensification of the subtropical jets (Fig. 6), as reported in the literature (e.g., Seager et al. 2003; Lu et al. 2008; Calvo et al. 2010).
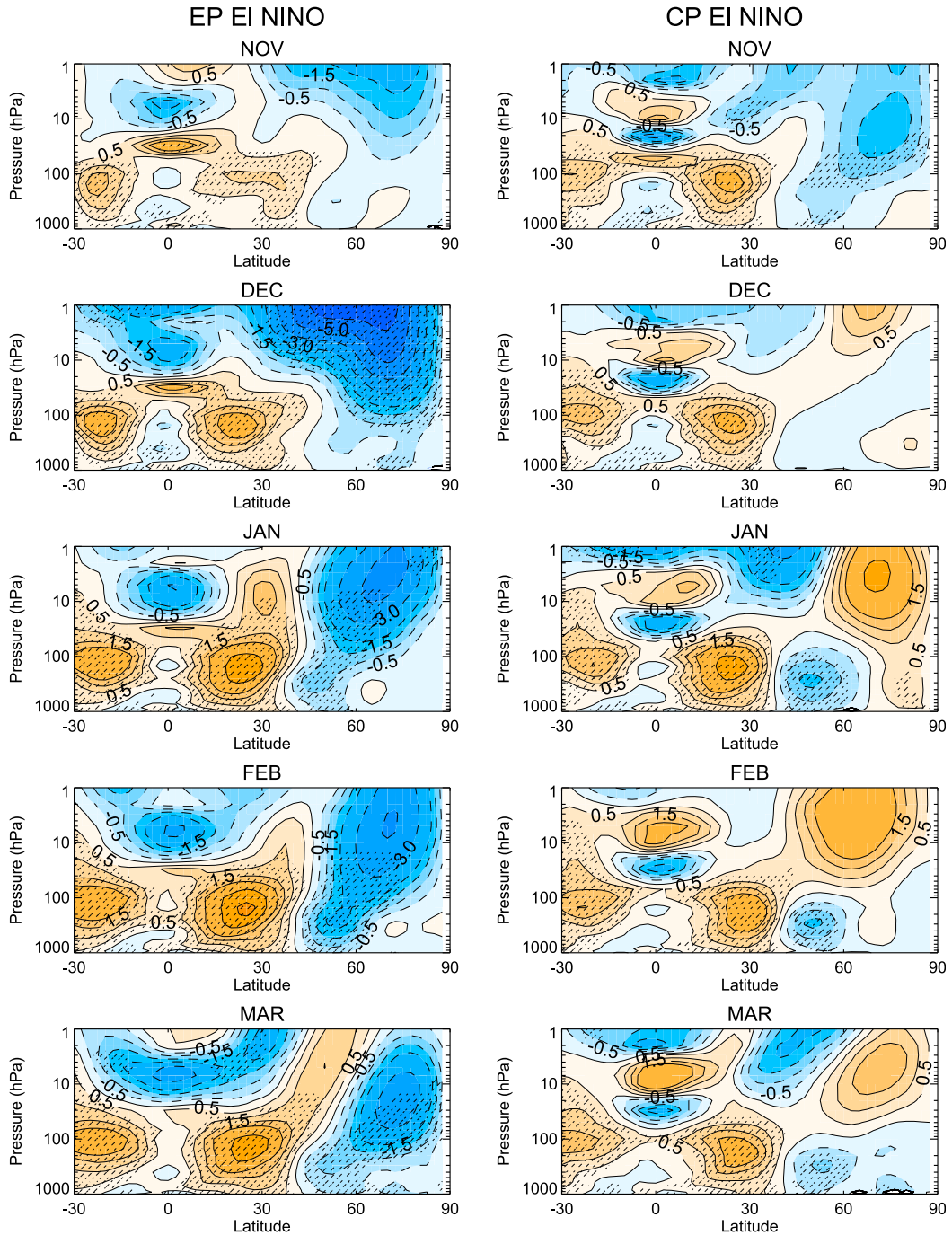
FIG. 6. As in Fig. 5, but for zonal-mean zonal wind anomalies (m s^{-1}). Contour interval is 0.5 m s^{-1} up to 2 m s^{-1} and 1 m s^{-1} for values above 2 m s^{-1}.

In the NH polar region, a robust warming appears during EP El Niño in November in the upper stratosphere; it intensifies in December and moves downward toward the lower polar stratosphere from January to March. The largest anomalies range from 2 to 3.5 K throughout the winter. Consistently, significant easterly wind anomalies

are simulated in November in the upper stratosphere at middle and high latitudes, weakening the polar vortex from December to March. Similar zonal-mean signals were present in previous studies (e.g., García-Herrera et al. 2006; Manzini et al. 2006) and are in agreement with the wave1 intensification and constructive interference between

wave1 EP El Niño anomalies and the climatology, as shown in Figs. 3 and 4. In contrast, the CP El Niño events do not show a robust response in the polar region in either zonal-mean temperature or zonal-mean zonal wind anomalies from December to March. These results are consistent with the weaker and delayed tropospheric PNA response found in CP events (Fig. 2) and the lack of constructive interference between the waves and climatology until February (Figs. 3, 4). Note that, even though there are positive wave1 eddy heat flux values in this month during CP events (indicative of constructive interference), there is not a significant response in zonal-mean temperature or wind, but there is a tendency toward less cooling and less strengthening of the polar stratosphere between February and March. Overall, the CMIP5 patterns in temperature and zonal wind are in remarkably good agreement with NCEP–NCAR reanalyses results from Sung et al. (2014) and Iza and Calvo (2015).

In addition to the polar stratospheric anomalies, Fig. 6 shows that, during EP events, significant easterly wind anomalies descend toward the troposphere and reach the surface mainly in February and March. During CP events, the nonsignificant signals at the polar region do not extend toward the troposphere. Differences in the seasonal evolution of the downward propagation of the polar signals between EP and CP El Niño events can be compactly illustrated by plotting the October–March zonal-mean zonal wind averaged between 45° and 75°N as a function of altitude (Figs. 7a,b), following the diagnostic first used by Manzini et al. (2006). Other latitudinal averages around 60°N show similar results. Significant easterly zonal-mean zonal wind anomalies (up to $-6 \, \mathrm{m \, s^{-1}}$) are simulated during EP events in the upper polar stratosphere in December. They reach the troposphere in January and extend to the surface from February to April (negative anomalies up to $-0.5 \, \mathrm{m \, s^{-1}}$ at the surface). This is in agreement with the behavior reported from observations and previous results from atmospheric models driven with observed SSTs (Cagnazzo and Manzini 2009; Ineson and Scaife 2009; Bell et al. 2009). In contrast, such a development of a stratospheric anomaly propagating downward into the troposphere is not found for the CP events. In this case, not significant westerly anomalies are simulated in the stratosphere. Disconnected from the stratospheric behavior, weak significant easterly anomalies occur only in the troposphere from January to March.

Several studies have reported contradictory results in response to CP El Niño events in observations (see, e.g., Garfinkel et al. 2013), which Iza and Calvo (2015) attributed to the occurrence of SSWs. The role of SSWs in the CMIP5 El Niño response is addressed here by considering EP and CP El Niño winters with and without

SSWs. Figures 7c and 7d show the EP and CP composites with SSWs, respectively, while Figs. 7e and 7f are for the EP and CP composites without SSWs. Interestingly, during EP El Niño events, a weaker polar vortex is simulated in the upper stratosphere in December regardless of the occurrence of SSWs (Figs. 7c,e). However, this response propagates downward only during EP El Niño winters with SSWs, with the largest values reaching the surface in February. In the absence of SSWs in the EP El Niño composite (Fig. 7e), the upper-stratospheric easterly wind anomaly in December does not propagate into the troposphere. These differences in the EP El Niño signal highlight the role of SSWs in propagating the signal toward the troposphere, in agreement with previous single-model studies (Cagnazzo and Manzini 2009; Ineson and Scaife 2009).

During CP El Niño winters with SSWs (Fig. 7d), a significant easterly anomaly appears in the middle stratosphere in February and March and in the troposphere from January to March. In the absence of SSWs, a significant strengthening of the stratospheric polar vortex is found in February and March, in agreement with reanalysis results from Iza and Calvo (2015).

The different behavior during winters with and without SSWs shown in Figs. 7c–f might arise because the anomalies are computed with respect to a mean climatology that includes all years of each model simulation, generally colder than the mean of winters with SSWs and warmer than the mean of winters without SSWs. Thus, to test the sensitivity of the EP and CP responses with and without SSWs to the mean state, Fig. 8 shows the downward propagation of EP and CP El Niño zonal-mean zonal wind anomalies computed as explained next. For each El Niño event, the anomalies are computed with respect to their own model climatology of years with and without SSWs; then El Niño anomalies are composited. During EP El Niño events (Figs. 8a,c), easterly anomalies are simulated in early winter (from November to January) in the stratosphere, and they propagate downward regardless of the occurrence of SSWs. However, the tropospheric signal is stronger and robust in EP winters with SSWs. In the middle stratosphere, statistical significance is generally lost in the EP El Niño case with SSWs, probably because of the large polar stratospheric variability in the climatology of winters with SSWs. During CP El Niño events, the wind anomalies are instead not consistent in the composites with and without SSWs, as their sign depends on the specific case considered (Figs. 8b,d).

These results indicate that the EP stratospheric El Niño response (an anomalous weaker polar vortex and warmer polar stratosphere) is robust in early winter regardless of the occurrence of SSWs, although SSWs
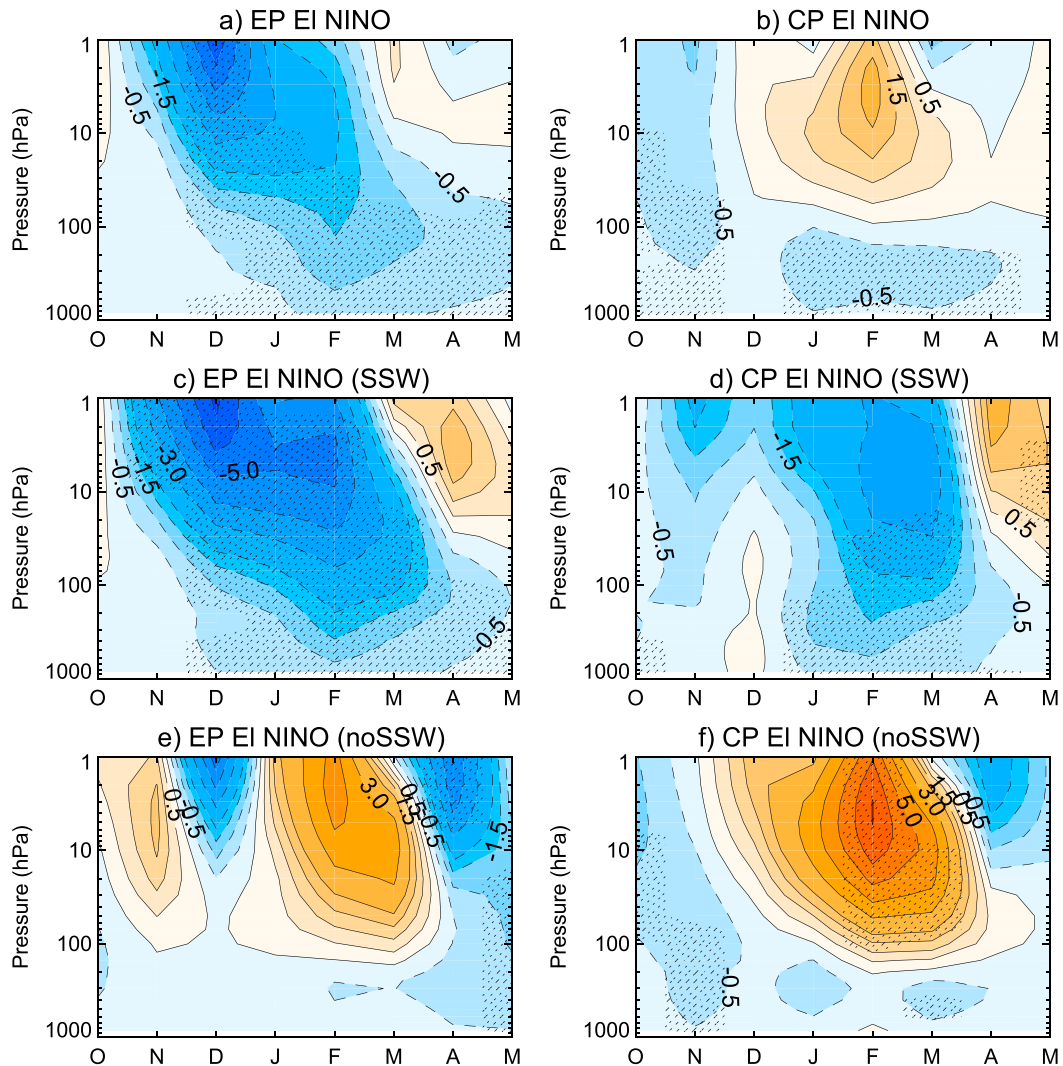
FIG. 7. Month–pressure cross section of the 45°–75°N average zonal-mean zonal wind anomalies (m s^{-1}) composited for (a) EP El Niño and (b) CP El Niño; (c),(d) for EP and CP El Niño winters with SSWs, respectively; and (e),(f) for EP and CP El Niño winters without SSWs, respectively. The number of winters included in each composite is shown in Table 2. Contour intervals are 0.5 m s^{-1} up to 2 m s^{-1} and 1 m s^{-1} for larger values. Solid (dashed) contours denote positive (negative) anomalies. Stippling indicates significance at the 95% confidence level.

seem to favor the downward propagation of the signal toward the surface in late winter. In addition, Table 2 shows that there is likely a preference for SSWs to occur during EP El Niño events (32 winters with SSWs out of 48 total EP El Niño winters vs 20 winters with SSWs out of 43 total CP El Niño winters). The frequency of occurrence of SSWs during EP El Niño winters is indeed 67%, statistically different from the SSW climatological frequency (52% for the entire 594 yr considered) at the 95% confidence level. On the other hand, the frequency of occurrence of SSWs during CP El Niño winters is 46%, which is not statistically different from climatological values at the 95% confidence level. In both cases,

the significance was tested with a Monte Carlo test of 1000 trials. The number of SSWs in EP or CP El Niño winters was tested against random groups of 48 and 43 winters, respectively, extracted from the entire pool of all winters from all the models. The statistically significant larger frequency of SSWs during EP El Niño is in agreement with previous modeling studies (e.g., Taguchi and Hartmann 2006; Cagnazzo and Manzini 2009) and indicates that both EP El Niño and SSWs are nonlinearly related. Note that the higher frequency of SSWs for EP El Niño leads to an ensemble of EP El Niño winters without SSW, which is indeed half the size of that with SSWs (16 cases; see Table 3). Thus, composites
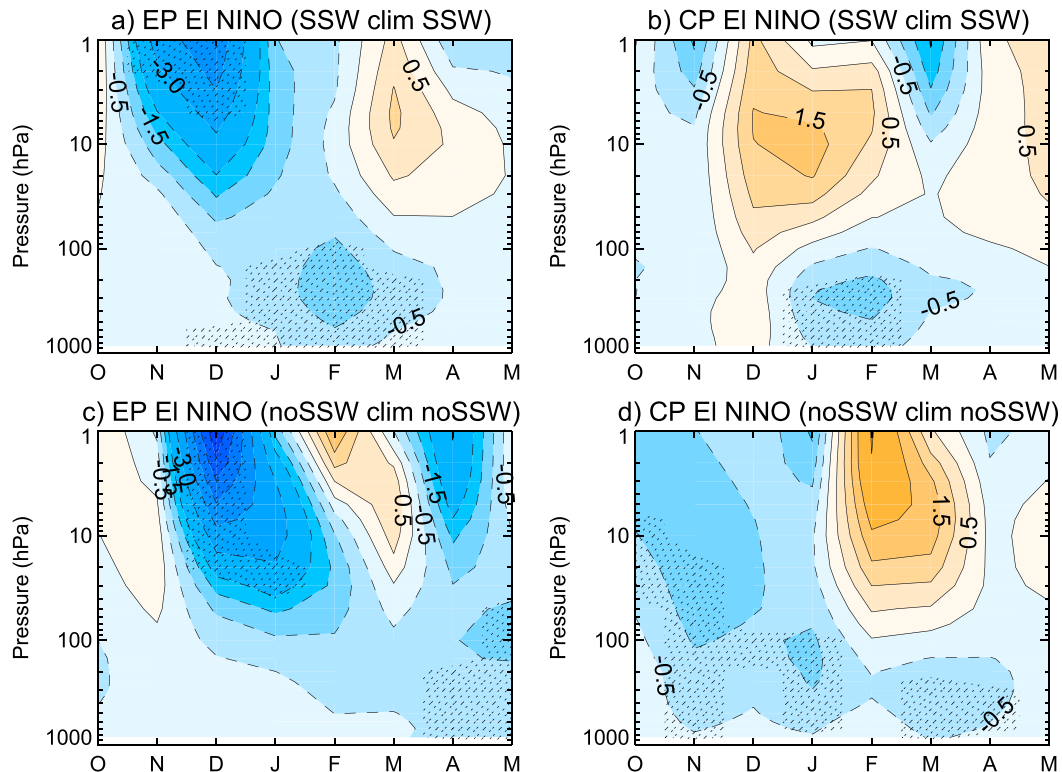
FIG. 8. (a),(b) As in Figs. 7c and 7d, but for EP and CP El Niño winters with SSWs, with anomalies computed with respect to the multimodel mean climatology of winters with SSWs (a total of 307 winters). (c),(d) As in Figs. 7e and 7f, but for EP and CP El Niño winters without SSWs, with anomalies computed with respect to the multimodel mean climatology of winters without SSWs (a total of 287 winters). See more details in the text for the calculation of the anomalies. Contour intervals are $0.5\,\mathrm{m\,s^{-1}}$ up to $2\,\mathrm{m\,s^{-1}}$ and $1\,\mathrm{m\,s^{-1}}$ for larger values. Solid (dashed) contours denote positive (negative) anomalies. Stippling indicates significance at the 95% confidence level.

from this latter subset need to be considered with more caution, as they might be less robust than those for EP El Niño winters with SSWs. The insignificant change in the frequency of occurrence of SSWs during CP winters could be the reason for the lack of robustness (e.g., inconsistency in sign and pattern) in the stratospheric response to CP El Niño.

We have shown zonal-mean differences throughout the winter season in the polar stratosphere and downward propagation in relation to the occurrence of SSWs. We have recalculated the phase difference between the anomalous El Niño wave1 and the climatological wave1 (as in Fig. 3, right) and the wave1 eddy heat flux anomalies (as in Fig. 4) for EP and CP El Niño winters with and without SSWs (not shown). Within the troposphere and in early winter (November–December, the period with upward dynamical coupling from the troposphere to the stratosphere), the EP El Niño phase anomalies stay close to zero, indicating an in-phase relationship (as in Fig. 3, right) regardless of the occurrence of SSWs. In the

case of CP El Niño events, there is less consistent in-phase behavior in the troposphere. In early winter, CP El Niño phase anomalies are close to zero only in December for winters with SSWs. The wave1 eddy heat flux anomalies are consistent with Fig. 7, showing larger values in winters with SSWs, for both EP and CP El Niño events.

6. Role of the stratosphere on the tropospheric El Niño teleconnections in the North Atlantic–European region

Growing evidence shows the impact that downward-propagating anomalies from the polar stratosphere into the troposphere have on tropospheric climate in the North Atlantic–European region during El Niño events (e.g., Cagnazzo and Manzini 2009; Ineson and Scaife 2009; Butler et al. 2014). The differences between EP and CP events shown previously are therefore expected to lead to differences in surface signals. This is explored in Figs. 9a and 9b, which show the CMIP5 sea level

SLP

a) EP El NINO

b) CP El NINO

[hPa]

-12 -11 -10 -9 -8 -7 -6 -5 -4 -3 -2 -1 0 1 2 3 4 5 6 7 8 9 10 11

TS

c) EP El NINO

d) CP El NINO

[K]

-5.0 -4.5 -4.0 -3.5 -3.0 -2.5 -2.0 -1.5 -1.0 -0.5 0.0 0.5 1.0 1.5 2.0 2.5 3.0 3.5 4.0 4.5
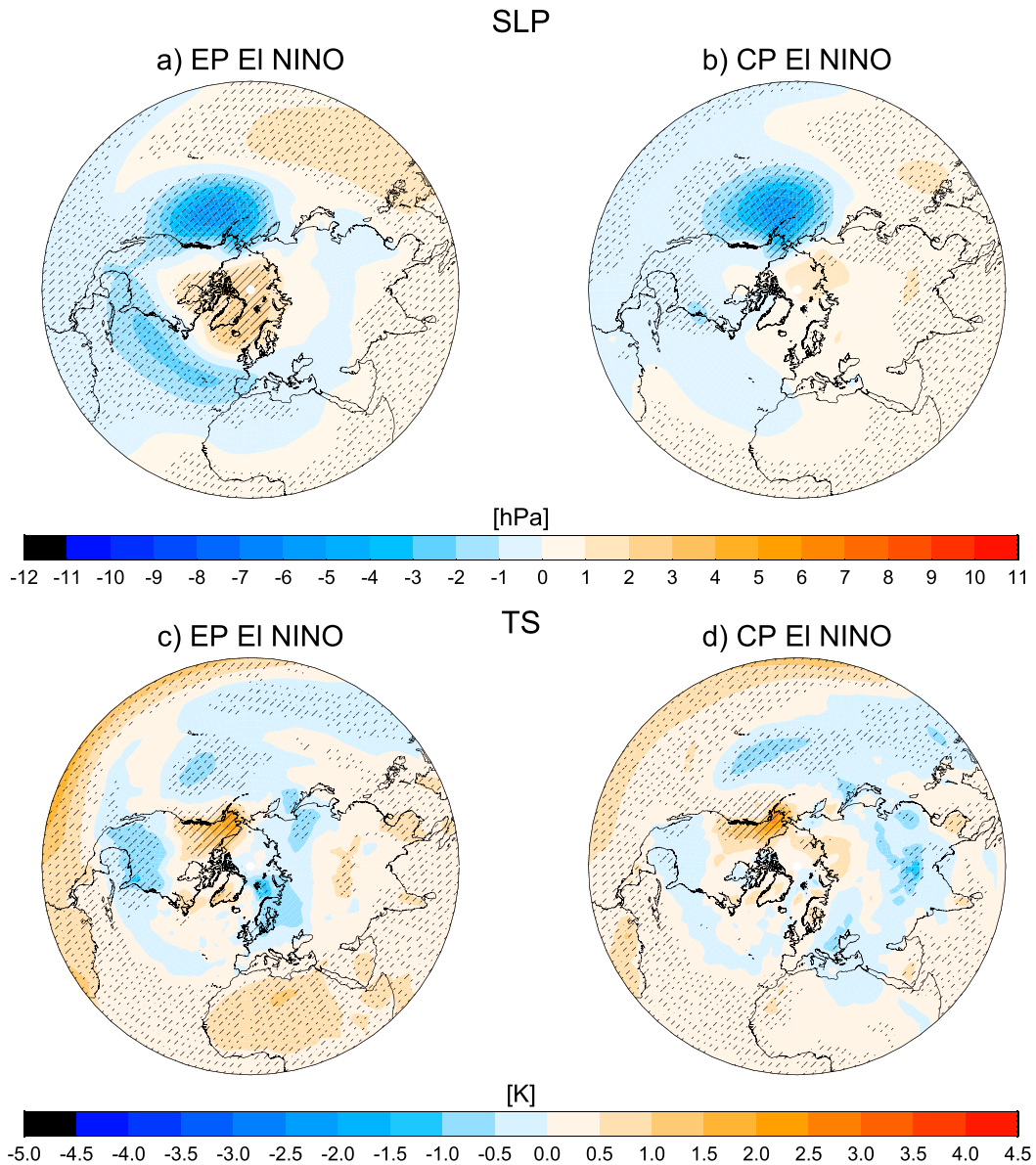
FIG. 9. Northern Hemisphere February–March averages of (top) SLP and (bottom) surface temperature anomalies composited for (left) EP El Niño and (right) CP El Niño. Stippling indicates significance at the 95% confidence level.

pressure anomalies composited for EP and CP El Niño events in February and March, when the largest tropospheric responses are simulated. During EP El Niño events, the sea level pressure (SLP) pattern displays a clear and robust negative AO structure, with positive anomalies over the polar cap and negative anomalies in the middle latitudes centered in the Pacific and Atlantic Oceans. Although the negative anomalies over the North Pacific appear throughout the winter (from November to March, not shown), the strong robust positive anomaly over the polar cap and the negative anomaly

over the Atlantic and Europe are only simulated in February and March. This is in excellent agreement with results from single-model studies that used observed SSTs as boundary conditions with many ensemble members, from mechanistic simulations, and from observations (Ineson and Scaife 2009; Cagnazzo and Manzini 2009; Bell et al. 2009; Butler et al. 2014). During CP El Niño events, a robust negative sea level pressure anomaly is simulated in the North Pacific. However, the response over the polar cap and the NAE region (giving the annular pattern) is not developed during any month

(not shown). The absence of a substantial response in the NAE region for CP events is consistent with the weak and not robust signal simulated in the stratosphere by the CMIP5 models and the lack of downward propagation reported in the previous section.

The patterns in sea level pressure are in agreement with the signals in surface temperature (Figs. 9c,d). Significant warmer temperatures are simulated over Canada and colder temperatures over the United States and Mexico in both EP and CP events. This response is robust throughout the winter, consistent with the negative anomalies in SLP in the northern Pacific Ocean and deepening of the Aleutian low. This suggests the response does not come from the stratosphere but it is part of the tropospheric PNA teleconnection, as also discussed by Butler et al. (2014). During EP events, significant cold anomalies are simulated in February and March in northern and central Europe and Siberia, consistent with the negative phase of the AO driven by the stratospheric EP El Niño signal. This pattern is also known to be associated with anomalous easterly zonal winds at the surface and a reduction of the warm air advection from the North Atlantic Ocean to northern and central Europe (e.g., Cagnazzo and Manzini 2009). During CP El Niño events, no signal is simulated in this region supporting the lack of any stratospheric influence in this case.

In the previous section, we also assessed the influence of SSWs in the downward propagation of the EP and CP El Niño signals. Next, we investigate the tropospheric NAE teleconnections in sea level pressure and surface temperature stratifying according to the occurrence of SSWs (Figs. 10, 11). Results are very similar regardless of the climatology used to compute the anomalies. A negative AO phase is simulated in both EP and CP El Niño winters with SSWs in the February–March average, although the response over the pole and the Atlantic Ocean and Europe is stronger, more robust, and significant over larger areas in EP events. Consequently, the surface temperature response is quite different over northern Europe in EP and CP events (Figs. 11a,b). While it shows a strong significant cooling in response to EP El Niño winters with SSWs, the signal in sea level pressure in the case of CP El Niño does not seem to be strong enough to drive large significant temperature anomalies via anomalous surface winds.

In the absence of SSWs, the SLP response to EP El Niño events resembles that during EP El Niño winters with SSWs, although the anomalies over the pole are very weak and hardly significant. This is in agreement with the weaker and not significant zonal-mean zonal wind anomalies in Figs. 7e and 8c and the lack of significant signal over Europe in surface temperature

(Fig. 11c). These differences between EP El Niño winters with and without SSWs reflect the role of SSWs in driving the tropospheric EP El Niño signal. This, together with the significantly enhanced occurrence of SSWs during EP El Niño winters shown in the previous section, indicates that the surface response to SSWs and EP El Niño events are difficult to address separately. Finally, during CP El Niño events without SSWs, only the significant negative anomaly over the North Pacific (Fig. 9d), reminiscent of the enhancement of the Aleutian low, and the corresponding anomalous warming over western Canada and Alaska (Fig. 11d) are simulated.

7. Summary and discussion

The seasonal evolution of the NH stratospheric signals in response to two different flavors of El Niño—the eastern Pacific El Niño and the central Pacific El Niño—have been explored for the first time in an ensemble of simulations from atmosphere–ocean coupled models with a well-resolved stratosphere (the high-top CMIP5 historical simulations). The 11 CMIP5 models used here allowed for large composites, 48 EP events and 43 CP events, to address some of the uncertainties in the observational record commonly related to the small number of events considered (see, e.g., Garfinkel et al. 2013). The role of the stratosphere in driving tropospheric El Niño teleconnections in the NAE region in late winter and early spring has also been investigated.

The CMIP5 models reproduce the well-known behavior of EP El Niño in the NH (e.g., García-Herrera et al. 2006; Garfinkel and Hartmann 2008; Cagnazzo and Manzini 2009; Free and Seidel 2009; Ineson and Scaife 2009). The EP El Niño signal in the troposphere propagates from the tropics to the extratropics in the form of Rossby waves intensifying the positive phase of the PNA pattern. A robust deepening of the Aleutian low and an enhancement of the high over eastern Canada are simulated from November to February. This tropospheric pattern intensifies the climatological wave1, which propagates upward into the stratosphere through constructive interference and weakens the climatological wave2 pattern. Upward-propagating waves dissipate, decelerate the polar vortex, and warm the polar stratosphere. Then the anomalous zonal-mean wind anomalies propagate downward from the upper stratosphere into the troposphere and surface in February–March, having a simultaneous robust negative AO imprint in sea level pressure and surface temperature.

During CP El Niño winters, the CMIP5 models simulate a positive PNA pattern that is generally weaker and maximizes later in the winter compared to EP
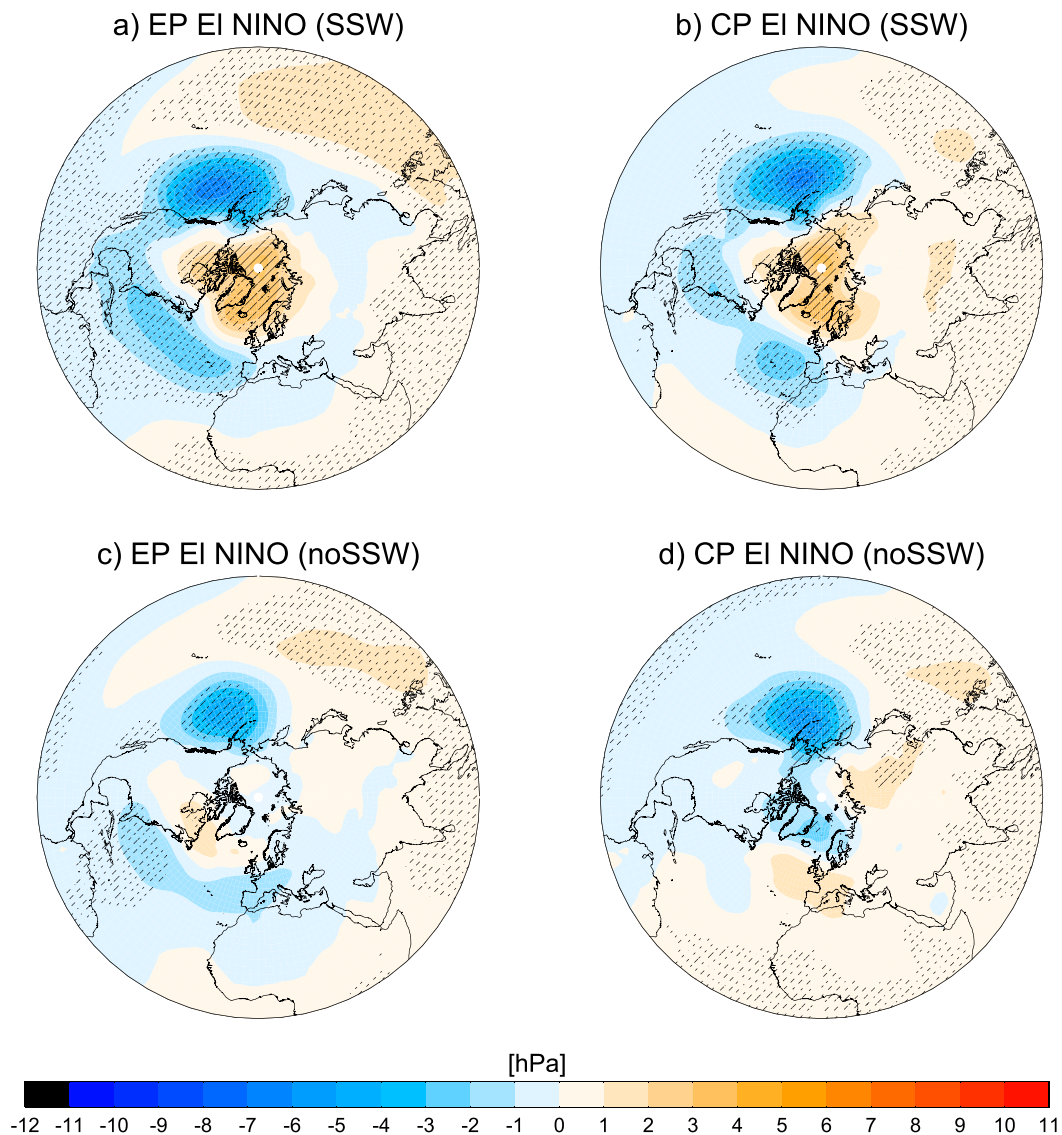
SLP

FIG. 10. Northern Hemisphere February–March averages of SLP anomalies composited for (a),(c) EP El Niño and (b),(d) CP El Niño for (top) winters with SSWs and (bottom) winters without SSWs. Anomalies are computed with respect to the entire multimodel mean climatology (similar to Fig. 7). Stippling indicates significance at the 95% confidence level.

El Niño. Intensification of the climatological wave1 through constructive interference in the lower stratosphere only occurs in February during CP El Niño events and so lacks the early winter upward wave propagation that occurs in response to EP events. This might be because the stratospheric pathway and its downward impact on the troposphere require a delay of about one to two months (Newman et al. 2001). As a result, the CMIP5 response to CP El Niño in the polar stratosphere is weak and not significant. This is

significantly different from EP events at the 95% confidence level from December to February. Also different from EP El Niño, the CP El Niño stratospheric response in CMIP5 models does not propagate downward into the troposphere and so does not affect surface climate in the NAE region.

Our results from CMIP5 models confirm previous suggestions from reanalysis (Sung et al. 2014) in that differences between EP and CP El Niño signals in the polar stratosphere are due to differences in the timing of the
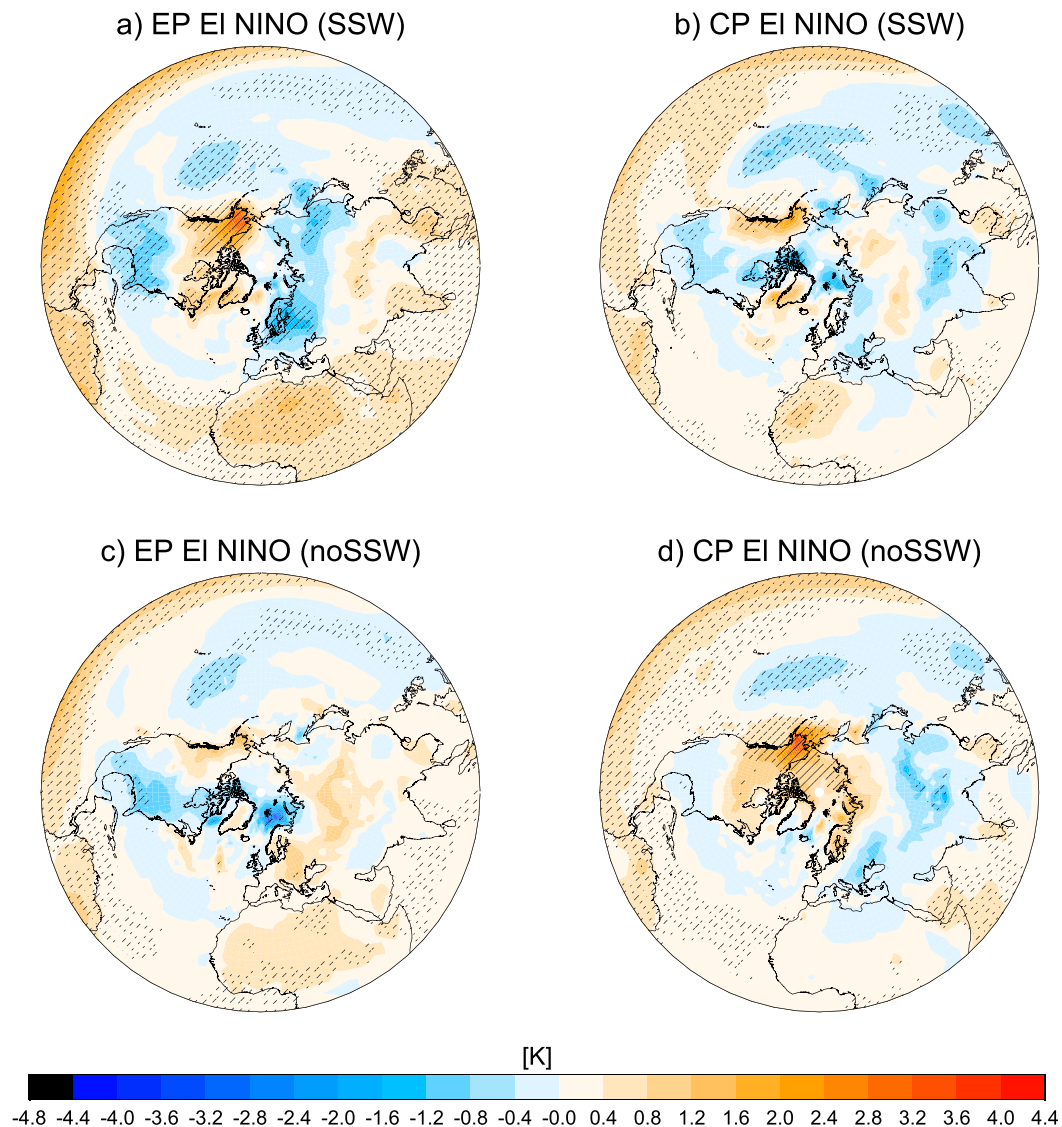
TS

FIG. 11. As in Fig. 10, but for surface temperature anomalies.

intensification of the PNA tropospheric teleconnection with respect to the seasonal cycle. Previous studies showed that these differences are associated with the different location of tropical convection anomalies between EP and CP events (e.g., Hurwitz et al. 2011a; Zubiaurre and Calvo 2012) and the extratropical background state (Branstator 2002; Frederiksen and Branstator 2005). In particular, CMIP5 models show an enhancement of the Aleutian low at higher latitudes in EP than in CP events in early winter, which supports earlier results by Garfinkel et al. (2013). Their idealized model simulations revealed that the northward displacement of the Aleutian low toward the Bering Strait enhanced

upward wave propagation into the stratosphere. In addition, we have shown that not only the deepening of the Aleutian low but also the intensification of the high over eastern Canada and its eastward extension (which has not received so much attention in the literature) are key for enhancing planetary wave1 and explain the differences between EP and CP stratospheric signals.

In the stratosphere, CMIP5 high-top models corroborate the previously reported response to EP El Niño in reanalysis data and atmosphere-only models: that is, a warmer polar stratosphere and weaker polar vortex. CMIP5 results also shed light on the contradictory responses to CP El Niño events. The negligible signal

during CP events on polar stratospheric temperatures and zonal-mean zonal winds is in agreement with reanalysis results from Garfinkel et al. (2013) and Iza and Calvo (2015). Even though the idealized single-model results of Garfinkel et al. (2013) indicated that large composites are needed to get a significant response to CP El Niño, the present CMIP5 results reveal a lack of response even when large composites are used. Our interpretation is that the absence of response is mainly due to the seasonally late establishment of El Niño teleconnection in the Pacific and because the frequency of occurrence of SSWs is not enhanced during CP events.

Our study also confirms the role of the polar stratosphere in driving tropospheric changes in the polar and NAE region during EP El Niño events in the form of a negative AO pattern. A weaker polar vortex appears in early winter in the polar upper stratosphere during EP El Niño regardless of the SSWs occurrence. However, only during EP winters with SSWs, the wind response reaches the surface, generating a stronger and significant negative AO pattern in the NH, in agreement with observations and previous modeling results that used atmospheric models run with observed SSTs. The significant enhanced frequency of SSWs during EP El Niño winters implies a nonlinear relationship between EP EL Niño and SSWs, with SSWs favored during EP El Niño. To separate the surface climate effects of the EP EL Niño and SSWs is, in turn, complicated and possibly somewhat ill posed (Polvani et al. 2016). In contrast, CMIP5 results show that the CP El Niño signal plays a negligible role in driving both the stratospheric pathway and, consequently, its tropospheric teleconnections in the NAE region. In fact, during CP events, the stratospheric response is the opposite in winters with and without SSWs, in agreement with reanalysis results (Iza and Calvo 2015). Only during CP El Niño winters with SSWs do the CMIP5 models simulate a negative AO pattern at the surface, although the coupling to the surface is weaker than during EP El Niño winters, particularly over Europe. This seems to be more related to the occurrence of SSWs than to the effect of CP events, as revealed by the frequency of occurrence of SSWs, which is not statistically different from the climatology in this case (at the 95% confidence level). This indicates that CP El Niño does not favor a perturbed stratosphere, whose most extreme manifestations are SSWs.

Therefore, the above analysis of the EP and CP El Niño events supports the relevance of correctly modeling the stratospheric responses to potentially improve climate predictability over Europe (Sigmond et al. 2013; Domeisen et al. 2015). However, according to our results from CMIP5 high-top models, only EP El Niño events show a nontrivial connection to SSWs and

consequently have the potential to enhance climate predictability in the NAE region via the stratospheric pathway.

Finally, we want to stress the importance of studying the seasonal evolution of EP and CP El Niño anomalies to understand similarities and differences between them and their remote impacts. Even though Hurwitz et al. (2014) did not find significant differences between the EP and CP seasonal-mean polar stratospheric response at 50 hPa in the high-top CMIP5 models, significant differences appear in the seasonal evolution of the monthly means throughout the stratosphere. Note that Hurwitz et al. (2014) did not find a significant correlation in CP events between their Walker cell or North Pole low minimum indices and the North Pole vortex weakening index, which is consistent with the not significant responses found here in the monthly mean behavior. In line with this, other interesting topics not addressed here are the seasonal evolution of La Niña stratospheric response in the CMIP5 models, its connection with SSWs (as observations and models seem to disagree in their frequencies), and the potential effects on NH tropospheric climate, as well as the quasi-biennial oscillation (QBO) modulation of the extratropical stratospheric signals of different flavors of ENSO. The enhanced frequency of SSWs during EP El Niño reported here and how exactly the EP El Niño–SSW link is established also deserves further investigation. Finally, the impact of El Niño flavors in the SH also needs to be clarified, as it has been proven to be significant during CP El Niño events in single-model studies and observations (Hurwitz et al. 2011a; Zubiaurre and Calvo 2012) but not in the seasonal means in CMIP5 models (Hurwitz et al. 2014). These topics will be hopefully explored in future studies.

REFERENCES

Ashok, K., S. K. Behera, S. A. Rao, H. Weng, and T. Yamagata, 2007: El Niño Modoki and its possible teleconnection. *J. Geophys. Res.*, **112**, C11007, doi:10.1029/2006JC003798.

Bell, C. J., L. J. Gray, A. J. Charlton-Perez, M. M. Joshi, and A. A. Scaife, 2009: Stratospheric communication of El Niño teleconnections to European winter. *J. Climate*, **22**, 4083–4096, doi:10.1175/2009JCLI2717.1.

Bellenguer, H., E. Guilyardi, J. Leloup, M. Lengaigne, and J. Vialard, 2014: ENSO representation in climate models: From CMIP3 to CMIP5. *Climate Dyn.*, **42**, 1999–2018, doi:10.1007/s00382-013-1783-z.

Branstator, G., 2002: Circumglobal teleconnections, the jet stream waveguide, and the North Atlantic Oscillation. *J. Climate*, **15**, 1893–1910, doi:10.1175/1520-0442(2002)015<1893: CTTJSW>2.0.CO;2.

Butler, A. H., L. M. Polvani, and C. Deser, 2014: Separating the stratospheric and tropospheric pathways of El Niño–Southern Oscillation teleconnections. *Environ. Res. Lett.*, **9**, 024014, doi:10.1088/1748-9326/9/2/024014.

Cagnazzo, C., and E. Manzini, 2009: Impact of the stratosphere on the winter tropospheric teleconnections between ENSO and the North Atlantic and European region. *J. Climate*, **22**, 1223–1238, doi:10.1175/2008JCLI2549.1.

——, and Coauthors, 2009: Northern winter stratospheric temperature and ozone responses to ENSO inferred from an ensemble of chemistry climate models. *Atmos. Chem. Phys.*, **9**, 8935–8948, doi:10.5194/acp-9-8935-2009.

Calvo, N., and D. R. Marsh, 2011: The combined effects of ENSO and the 11 year solar cycle on the Northern Hemisphere polar stratosphere. *J. Geophys. Res.*, **116**, D23112, doi:10.1029/2010JD015226.

——, M. A. Giorgetta, R. Garcia-Herrera, and E. Manzini, 2009: Nonlinearity of the combined warm ENSO and QBO effects on the Northern Hemisphere polar vortex in MAECHAM5 simulations. *J. Geophys. Res.*, **114**, D13109, doi:10.1029/2008JD011445.

——, R. R. Garcia, W. J. Randel, and D. R. Marsh, 2010: Dynamical mechanism for the increase in tropical upwelling in the lowermost tropical stratosphere during warm ENSO events. *J. Atmos. Sci.*, **67**, 2331–2340, doi:10.1175/2010JAS3433.1.

Calvo Fernández, N., R. R. García, R. García Herrera, D. Gallego Puyol, L. Gimeno Presa, E. Henández Martín, and P. Ribera Rodríguez, 2004: Analysis of the ENSO Signal in tropospheric and stratospheric temperatures observed by MSU, 1979–2000. *J. Climate*, **17**, 3934–3946, doi:10.1175/1520-0442(2004)017<3934: AOTESI>2.0.CO;2.

Charlton, A. J., and L. M. Polvani, 2007: A new look at stratospheric sudden warmings. Part I: Climatology and modeling benchmarks. *J. Climate*, **20**, 449–469, doi:10.1175/JCLI3996.1.

Charlton-Perez, A. J., and Coauthors, 2013: On the lack of stratospheric dynamical variability in low-top versions of the CMIP5 models. *J. Geophys. Res.*, **118**, 2494–2505, doi:10.1002/jgrd.50125.

Domeisen, D. I. V., A. H. Butler, K. Fröhlich, M. Bittner, W. A. Müller, and J. Baehr, 2015: Seasonal predictability over Europe arising from El Niño and stratospheric variability in the MPI-ESM seasonal prediction system. *J. Climate*, **28**, 256–271, doi:10.1175/JCLI-D-14-00207.1.

Fletcher, C. G., and P. J. Kushner, 2011: The role of linear interference in the annular mode response to tropical SST forcing. *J. Climate*, **24**, 778–794, doi:10.1175/2010JCLI3735.1.

Frederiksen, J. S., and G. Branstator, 2005: Seasonal variability of teleconnection patterns. *J. Atmos. Sci.*, **62**, 1346–1365, doi:10.1175/JAS3405.1.

Free, M., and D. J. Seidel, 2009: Observed El Niño–Southern Oscillation temperature signal in the stratosphere. *J. Geophys. Res.*, **114**, D23108, doi:10.1029/2009JD012420.

García-Herrera, R., N. Calvo, R. R. Garcia, and M. A. Giorgetta, 2006: Propagation of ENSO temperature signals into the middle atmosphere: A comparison of two general circulation models and ERA-40 reanalysis data. *J. Geophys. Res.*, **111**, D06101, doi:10.1029/2005JD006061.

Garfinkel, C. I., and D. L. Hartmann, 2008: Different ENSO teleconnections and their effects on the stratospheric polar vortex. *J. Geophys. Res.*, **113**, D18114, doi:10.1029/2008JD009920.

——, ——, and F. Sassi, 2010: Tropospheric precursors of anomalous Northern Hemisphere stratospheric polar vortices. *J. Climate*, **23**, 3282–3299, doi:10.1175/2010JCLI3010.1.

——, M. M. Hurwitz, D. W. Waugh, and A. H. Butler, 2013: Are the teleconnections of central Pacific and eastern Pacific El Niño distinct in boreal wintertime? *Climate Dyn.*, **41**, 1835–1852, doi:10.1007/s00382-012-1570-2.

Gerber, E. P., and Coauthors, 2012: Assessing and understanding the impact of stratospheric dynamics and variability on the Earth system. *Bull. Amer. Meteor. Soc.*, **93**, 845–859, doi:10.1175/BAMS-D-11-00145.1.

Graf, H.-F., and D. Zanchettin, 2012: Central Pacific El Niño, the "subtropical bridge," and Eurasian climate. *J. Geophys. Res.*, **117**, D01102, doi:10.1029/2011JD016493.

Hegyi, B. M., and Y. Deng, 2011: A dynamical fingerprint of tropical Pacific sea surface temperatures on the decadal-scale variability of cool-season Arctic precipitation. *J. Geophys. Res.*, **116**, D20121, doi:10.1029/2011JD016001.

——, ——, R. X. Black, and R. Zhou, 2014: Initial transient response of the winter polar stratospheric vortex to idealized equatorial Pacific sea surface temperature anomalies in the NCAR WACCM. *J. Climate*, **27**, 2699–2713, doi:10.1175/JCLI-D-13-00289.1.

Hurwitz, M. M., P. A. Newman, L. D. Oman, and A. M. Molod, 2011a: Response of the Antarctic stratosphere to two types of El Niño events. *J. Atmos. Sci.*, **68**, 812–822, doi:10.1175/2011JAS3606.1.

——, L. D. Oman, P. A. Newman, A. M. Molod, S. M. Frith, and J. E. Nielsen, 2011b: Events response of the Antarctic stratosphere to warm pool El Niño events in the GEOS CCM. *Atmos. Chem. Phys.*, **11**, 9659–9669, doi:10.5194/acp-11-9659-2011.

——, N. Calvo, C. I. Garfinkel, A. H. Butler, S. Ineson, C. Cagnazzo, E. Manzini, and C. Peña-Ortiz, 2014: Extratropical atmospheric response to ENSO in the CMIP5 models. *Climate Dyn.*, **43**, doi:10.1007/s00382-014-2110-z.

Ineson, S., and A. A. Scaife, 2009: The role of the stratosphere in the European climate response to El Niño. *Nat. Geosci.*, **2**, 32–36, doi:10.1038/ngeo381.

Iza, M., and N. Calvo, 2015: Role of stratospheric sudden warmings on the response to central Pacific El Niño. *Geophys. Res. Lett.*, **42**, 2482–2489, doi:10.1002/2014GL062935.

Kao, H.-Y., and J.-Y. Yu, 2009: Contrasting eastern-Pacific and central-Pacific types of ENSO. *J. Climate*, **22**, 615–632, doi:10.1175/2008JCLI2309.1.

Kim, H.-M., P. J. Webster, and J. A. Curry, 2009: Impact of shifting patterns of Pacific Ocean warming on North Atlantic tropical cyclones. *Science*, **325**, 77–80, doi:10.1126/science.1174062.

Kim, S. T., and J.-Y. Yu, 2012: The two types of ENSO in CMIP5 models. *Geophys. Res. Lett.*, **39**, L11704, doi:10.1029/2012GL052006.

Kug, J.-S., F.-F. Jin, and S.-I. An, 2009: Two types of El Niño events: Cold tongue El Niño and warm pool El Niño. *J. Climate*, **22**, 1499–1515, doi:10.1175/2008JCLI2624.1.

——, Y.-G. Ham, J.-Y. Lee, and F.-F. Jin, 2012: Improved simulation of two types of El Niño in CMIP5 models. *Environ. Res. Lett.*, **7**, 034002, doi:10.1088/1748-9326/7/3/034002.

Larkin, N. K., and D. E. Harrison, 2005: Global seasonal temperature and precipitation anomalies during El Niño autumn and winter. *Geophys. Res. Lett.*, **32**, L16705, doi:10.1029/2005GL022860.

Li, T., N. Calvo, J. Yue, X. Dou, J. M. Russell, M. G. Mlynczak, C.-Y. She, and X. Xue, 2013: Influence of El Niño–Southern Oscillation in the mesosphere. *Geophys. Res. Lett.*, **40**, 3292–3296, doi:10.1002/grl.50598.

Li, Y., and N. C. Lau, 2013: Influences of ENSO on stratospheric variability, and the descent of stratospheric perturbations into the lower troposphere. *J. Climate*, **26**, 4725–4748, doi:10.1175/JCLI-D-12-00581.1.

Lu, H., M. P. Baldwin, L. J. Gray, and M. J. Jarvis, 2008: Decadal-scale changes in the effect of the QBO on the northern stratospheric polar vortex. *J. Geophys. Res.*, **113**, D10114, doi:10.1029/2007JD009647.

Manzini, E., M. A. Giorgetta, M. Esch, L. Kornblueh, and E. Roeckner, 2006: The influence of sea surface temperatures on the northern winter stratosphere: Ensemble simulations with the MAECHAM5 model. *J. Climate*, **19**, 3863–3882, doi:10.1175/JCLI3826.1.

Newman, P. A., E. R. Nash, and J. E. Rosenfield, 2001: What controls the temperature of the Arctic stratosphere during the spring? *J. Geophys. Res.*, **106**, 19 999–20 010, doi:10.1029/2000JD000061.

Polvani, L. M., L. Sun, A. H. Butler, J. H. Richter, and C. Deser, 2016: Distinguishing stratospheric sudden warmings from ENSO as key drivers of wintertime climate variability over the North Atlantic and Eurasia. *J. Climate*, **30**, 1959–1969, doi:10.1175/JCLI-D-16-0277.1.

Richter, J. H., C. Deser, and L. Sun, 2015: Effects of stratospheric variability on El Niño teleconnections. *Environ. Res. Lett.*, **10**, 124021, doi:10.1088/1748-9326/10/12/124021.

Sassi, F., D. Kinnison, B. A. Boville, R. R. Garcia, and R. Roble, 2004: Effect of El Niño–Southern Oscillation on the dynamical, thermal, and chemical structure of the middle atmosphere. *J. Geophys. Res.*, **109**, D17108, doi:10.1029/2003JD004434.

Seager, R., N. Harnik, Y. Kushnir, W. Robinson, and J. Miller, 2003: Mechanisms of hemispherically symmetric climate variability. *J. Climate*, **16**, 2960–2978, doi:10.1175/1520-0442(2003)016<2960:MOHSCV>2.0.CO;2.

Sigmond, M., J. F. Scinocca, V. V. Kharin, and T. G. Shepherd, 2013: Enhanced seasonal forecast skill following stratospheric sudden warmings. *Nat. Geosci.*, **6**, 98–102, doi:10.1038/ngeo1698.

Smith, K. L., and P. J. Kushner, 2012: Linear interference and the initiation of extratropical stratosphere–troposphere interactions. *J. Geophys. Res.*, **117**, D13107, doi:10.1029/2012JD017587.

——, C. G. Fletcher, and P. J. Kushner, 2010: The role of linear interference in the annular mode response to extratropical surface forcing. *J. Climate*, **23**, 6036–6050, doi:10.1175/2010JCLI3606.1.

Sung, M.-K., B.-M. Kim, and S.-I. An, 2014: Altered atmospheric responses to eastern Pacific and central Pacific El Niños over the North Atlantic region due to stratospheric interference. *Climate Dyn.*, **42**, 159–170, doi:10.1007/s00382-012-1661-0.

Taguchi, M., and D. L. Hartmann, 2006: Increased occurrence of stratospheric sudden warmings during El Niño as simulated by WACCM. *J. Climate*, **19**, 324–332, doi:10.1175/JCLI3655.1.

Taylor, K. E., R. J. Stouffer, and G. A. Meehl, 2012: An overview of CMIP5 and the experiment design. *Bull. Amer. Meteor. Soc.*, **93**, 485–498, doi:10.1175/BAMS-D-11-00094.1.

Wallace, J. M., and D. S. Gutzler, 1981: Teleconnections in the geopotential height field during the Northern Hemisphere winter. *Mon. Wea. Rev.*, **109**, 784–812, doi:10.1175/1520-0493(1981)109<0784:TITGHF>2.0.CO;2.

Weng, H., K. Ashok, S. K. Behera, S. A. Rao, and T. Yamagata, 2007: Impacts of recent El Niño Modoki on dry/wet conditions in the Pacific Rim during boreal summer. *Climate Dyn.*, **29**, 113–129, doi:10.1007/s00382-007-0234-0.

——, S. K. Behera, and T. Yamagata, 2009: Anomalous winter climate conditions in the Pacific Rim during recent El Niño Modoki and El Niño events. *Climate Dyn.*, **32**, 663–674, doi:10.1007/s00382-008-0394-6.

Xie, F., J. Li, W. Tian, J. Feng, and Y. Huo, 2012: Signals of El Niño Modoki in the tropical tropopause layer and stratosphere. *Atmos. Chem. Phys.*, **12**, 5259–5273, doi:10.5194/acp-12-5259-2012.

Yeh, S.-W., J.-S. Kug, B. Dewitte, M.-H. Kwon, B. P. Kirtman, and F.-F. Jin, 2009: El Niño in a changing climate. *Nature*, **461**, 511–514, doi:10.1038/nature08316.

Yu, J.-Y., and S. T. Kim, 2011: Relationships between extratropical sea level pressure variations and the central Pacific and eastern Pacific types of ENSO. *J. Climate*, **24**, 708–720, doi:10.1175/2010JCLI3688.1.

Zubiaurre, I., and N. Calvo, 2012: The El Niño–Southern Oscillation (ENSO) Modoki signal in the stratosphere. *J. Geophys. Res.*, **117**, D04104, doi:10.1029/2011JD016690.